



Article

Comprehensive Analysis of PPP-B2b Service and Its Impact on BDS-3/GPS Real-Time PPP Time Transfer

Jian Tang ¹, Daqian Lyu ^{1,*}, Fangling Zeng ¹, Yulong Ge ² and Runzhi Zhang ³¹ College of Electronic Engineering, National University of Defense Technology, Hefei 230037, China² School of Marine Science and Engineering, Nanjing Normal University, Nanjing 210023, China³ National Time Service Center, Chinese Academy of Sciences, Xi'an 710600, China

* Correspondence: daqian_lv@nudt.edu.cn

Abstract: 2020 saw the official completion of the BDS-3 and the start of the PPP-B2b signal-based real-time precise point positioning (PPP) service to users in China and the neighboring areas. In this work, the quality of PPP-B2b products is first evaluated and compared with real-time products from the CNES and the differential code bias (DCB) from the Chinese Academy of Science (CAS). Then, a detailed performance evaluation of the PPP time transfer based on the PPP-B2b service (B2b-RTPPP) is conducted. Three solutions, namely, GPS-only (G), BDS-3-only (C), and GPS + BDS-3 (GC) B2b-RTPPP solutions, are compared and assessed. The results suggest that for the PPP-B2b products, BDS-3 satellites have better orbit and clock offset quality than GPS satellites, while the opposite is true for CNES products. The quality of the PPP-B2b orbit and clock offset is poorer than those of the CNES. The PPP-B2b DCB shows excellent agreement with the CAS DCB. The accuracy of the B2b-RTPPP solutions is sub-nanosecond level. The accuracy of B2b-RTPPP time transfer with DCB correction is approximately improved by 64% compared with that without DCB correction. The GC B2b-RTPPP solution has the greatest frequency stability, while G B2b-RTPPP solution has the poorest. Considering that the receiver may be blocked, the B2b-RTPPP time transfer performance is also evaluated at different cut-off elevation angles. As the angle increases, the B2b-RTPPP time transfer performance decreases. Additionally, the short-term frequency stability remains constant at different cut-off elevation angles, but deteriorates in the long term, especially when the angle is 40°.

Keywords: BDS-3; GPS; real-time PPP; PPP-B2b; time transfer

Citation: Tang, J.; Lyu, D.; Zeng, F.; Ge, Y.; Zhang, R. Comprehensive Analysis of PPP-B2b Service and Its Impact on BDS-3/GPS Real-Time PPP Time Transfer. *Remote Sens.* **2022**, *14*, 5366. <https://doi.org/10.3390/rs14215366>

Academic Editor: Yunbin Yuan

Received: 23 September 2022

Accepted: 24 October 2022

Published: 26 October 2022

Publisher's Note: MDPI stays neutral with regard to jurisdictional claims in published maps and institutional affiliations.



Copyright: © 2022 by the authors. Licensee MDPI, Basel, Switzerland. This article is an open access article distributed under the terms and conditions of the Creative Commons Attribution (CC BY) license (<https://creativecommons.org/licenses/by/4.0/>).

1. Introduction

The precise point positioning (PPP) technique has attracted much interest because of its advantages of being able to operate with a single receiver, being flexible, and being not limited by distance [1,2]. The PPP technique uses code and carrier phase measurements for time transfer [3]. Relying on the precise products released by international GNSS service (IGS), the accuracy of time transfer at the sub-nanosecond level can be achieved by PPP all over the world [4]. The PPP has been widely used in the fields of time-scale maintenance [5], atmospheric water vapor measurement [6], automated vehicle navigation [7], and ionospheric delay inversion [8] for many years. However, in the early stages, the PPP technique is only applicable to post-processing cases because of the long latency of the IGS final products.

Real-time scenarios, such as 5G communication [9], landslide monitoring [10], and precise timing [11], require shorter latency and higher quality orbit and clock offset products thanks to the continuous advancement of the PPP technique. The IGS started the Real-time Pilot Project in 2007 and launched real-time service (RTS) in 2013, attracting much attention from scholars. RTS products are broadcast in the Radio Technology Committee of Marine (RTCM) format via the NTRIP protocol, which enables real-time PPP for time transfer. Elsobeiey et al. assessed the PPP performance of IGS RTS products and verified their

superiority over IGS ultra-rapid products [12]. The mathematical models of real-time PPP were introduced by Liu et al. [10], and the positioning performance was assessed using raw observations. A novel method of real-time precise timing was improved by Ge et al. employing IGS products [13], and it was shown that the accuracy of the timing solutions can achieve 0.2 ns. However, real-time PPP using IGS RTS relies on the IGS real-time streams through the Internet, which may be disrupted by equipment failure or network outage. In this case, an obvious decline in PPP performance is possible. To solve this problem, some navigation systems provide differential corrections to the broadcast ephemeris, providing access to precise real-time products rather than products via the Internet. Nowadays, the Quasi-Zenith Satellite System can broadcast the centimeter-level augmentation services (CLAS) for Japanese users via the L6 signal [14], while the Galileo High Accuracy Service (HAS) can transmit corrections for GPS and Galileo users [15]. However, neither of them supports the BDS-3.

Under this background, BDS-3 was fully completed and officially launched the satellite-based augmentation service in October 2020 to enable the real-time PPP. The BDS-3 consists of three Geostationary Earth Orbit (GEO), 24 Medium Earth Orbit (MEO), and three Inclined Geosynchronous Orbit (IGSO) satellites, with three additional frequency signals, B1C (1575.42 MHz), B2a (1176.4 MHz), and B2b (1207.14 MHz), while retaining the B1I (1561.098 MHz) and B3I (1268.520 MHz) signals of BDS-2 [16]. BDS-3 satellites are installed with more accurate on-board clocks compared to BDS-2, which enables better PPP performance for BDS-3 [17]. The state space representation (SSR) messages are released via the B2b signal through the three BDS-3 GEO satellites, which are available for users in mainland China and its maritime regions, and even the rest of the world [18–21]. The PPP-B2b service can provide correction messages for GPS LNAV and BDS-3 CNAV1 broadcast ephemeris that contain satellite mask, orbit correction parameters, User Range Accuracy Index (URAI), differential code bias (DCB) correction, and clock correction parameters [22]. The Issue of Data (IOD), including the IOD of SSR (IOD SSR), IOD of pseudo-random noise mask (IODP), IOD of navigation (IODN), and the IOD of orbit and clock corrections (IOD Corr), is employed as a matching indicator to ensure the correct matching between corrections and broadcast ephemeris. Correction messages can be matched for use only if the IODs retrieved from these messages are consistent and the received PPP-B2b correction message is within the nominal validity period, as shown in Table 1. It is important to note that the nominal validity period recommends the time range to use each type of message, and the quality of the data cannot be guaranteed for the message beyond the nominal validity period. Over the last few years, several studies on the PPP-B2b service have been carried out. Lu et al. [23] developed a homemade receiver to collect and decode real-time correction messages to evaluate the PPP-B2b service. Yang et al. [24] proposed a PPP method using PPP-B2b signal and verified the replaceability of the PPP-B2b service for IGS RTS. Xu et al. [25] conducted an all-round evaluation of the PPP-B2b service using B1I/B3I and B1C/B2a ionospheric-free (IF) observations. They concluded that the precision of the orbit and clock offset is greatly improved by the PPP-B2b, and that real-time PPP after convergence can reach positioning accuracy up to the centimeter. This has the advantages of being highly flexible and independence from the ground communication network and analysis center. However, we note that their research on the PPP-B2b has mainly focused on positioning; the performance of real-time PPP time transfer based on the PPP-B2b service (hereinafter referred to as B2b-RTPPP) remains unknown. To fill this gap, it is important to fully investigate the B2b-RTPPP time transfer performance.

The paper starts with the quality evaluation of the PPP-B2b products. Then, the B2b-RTPPP time transfer with combinations of different GNSS systems is studied. The detailed organization of this paper is as follows. We briefly describe the recovery strategies of precise orbits and clock offsets and introduce the principle of B2b-RTPPP time transfer in Section 2. In Section 3, experimental PPP-B2b data and its processing strategies are introduced. We assess the quality of the PPP-B2b orbit, clock offset, and DCB compared with the CNES products from and the CAS DCB, respectively in Section 4. The performance

of B2b-RTPPP time transfer is also analyzed. Finally, the conclusions and prospects of this paper are given in Section 5.

Table 1. Information of PPP-B2b messages.

Information Content	Message Type	IODs	Nominal Validity(s)
Clock correction	4, 6, 7	IOD SSR, IODP, IOD Corr	12
DCB correction	3	IOD SSR	86,400
Orbit correction	2, 6, 7	IOD SSR, IODN, IOD Corr	96
URAI	2, 5, 6, 7	-	96
Satellite mask	1	IOD SSR, IODP	-

2. Methods

In this section, the correction strategies of the precise real-time PPP-B2b orbit and clock offset are presented, along with the methods for evaluating the accuracy of PPP-B2b orbits, clock offsets, and DCB corrections. In addition, the B2b-RTPPP time transfer mode is proposed.

2.1. Assessment Methods of PPP-B2b Corrections

Currently, the PPP-B2b contains only the first four message types, as shown in Table 1. The IOD SSR represents the issue number of state space representation, which should remain consistent with each other for different message types. The IODP included in message types one and four denotes the satellite mask's data issue number. Users can use it to determine if the data in the two message types match. The ephemeris and clock offset corrections broadcast by the GNSS downlink signal are identified by the issue number IODN, and the users could determine whether the broadcast ephemeris matches the orbit corrections in message types two, six, and seven by the IODN. For shared satellites, they can be used to recover real-time orbits and clock offsets only if the clock offset's IOD Corr and the orbit's IOD Corr contained in message types two and four, respectively, are the same. The update periods of the two IOD Corrs are 48 s and 6 s. Note that when the clock offset's IOD Corr at the current moment is different from that at the previous moment, the orbit's IOD Corr does not change, which may lead to outliers in PPP. To eliminate the mismatching problem, when the two IOD Corrs are different, it is an efficient method to use the clock offset's IOD Corr that previously matched the orbit's IOD Corr, which will reduce the impact on the PPP performance [25].

Since the broadcast ephemeris provides the orbit corrections in the X/Y/Z components under the ECEF framework, and the PPP-B2b provides the orbit corrections in the radial (R), along-track (A), and cross-track (C) components, PPP-B2b satellite orbit corrections in the R/A/C directions should be converted to the corrections in the X/Y/Z directions under the ECEF coordinate system. The precise satellite orbit \mathbf{X}_{prec} and clock offset t_{prec} can be expressed by using Equations (1)–(3) [22].

$$\delta\mathbf{X} = [\mathbf{e}_r \quad \mathbf{e}_a \quad \mathbf{e}_c] \cdot \delta\mathbf{O} \quad (1)$$

$$\mathbf{X}_{prec} = \mathbf{X}_{brdc} - \delta\mathbf{X} \quad (2)$$

$$t_{prec} = t_{brdc} - \frac{C_0}{c} \quad (3)$$

where $\delta\mathbf{O} = [\delta O_r \quad \delta O_a \quad \delta O_c]^T$ is the vector of orbit parameters provided by PPP-B2b; $[\mathbf{e}_r \quad \mathbf{e}_a \quad \mathbf{e}_c]$ is an orthogonal matrix consisting of three unit vectors; $\delta\mathbf{X}$ is the converted vector of the orbit parameters; \mathbf{X}_{brdc} and t_{brdc} indicate the satellite coordinates and clock offsets obtained from the broadcast ephemeris, respectively; C_0 is the PPP-B2b clock parameters; and c is the speed of light in the vacuum.

In addition, the DCB caused by the hardware delay difference of the satellites between different frequencies could affect the PPP performance. The PPP-B2b provides the DCB products to eliminate the hardware delay and enable synchronous processing of different signals by using the Equation (4) [22].

$$\tilde{P}_{sig} = P_{sig} - DCB_{sig} \quad (4)$$

where P_{sig} is the initial observations; DCB_{sig} denotes the differential code bias of the corresponding signal; and \tilde{P}_{sig} denotes the corrected observations.

Since there are more than 120 global monitoring stations to calculate the GeoForschungZentrum (GFZ) multi-GNSS final product (GBM) using the B1I/B3I IF observations of a three-day arc, which can provide high accuracy of orbit and clock offset, the GBM final product is taken as the reference. With the GBM final products as a reference of comparison, the quality of the PPP-B2b orbit and clock offset products is assessed. The following issues must be considered. First, the PPP-B2b products provide satellite positions with the antenna phase center (APC) of B1I signal as a benchmark, while the GBM final product provides satellite positions in terms of the center of mass (CoM) [26]. Therefore, phase center offset (PCO) modifications are required to unify the satellite positions to the CoM using the “igs14.atx” file. It should be noted that the antenna file contains only the BDS-3 satellite antennas’ PCO and not the phase center variation. Second, the PPP-B2b product takes the B3I signal as the reference for the BDS-3 satellite clock offset, while the GBM final clock offset product takes the B1I/B3I IF signal as the reference. Therefore, the PPP-B2b DCB should be used to unify the BDS-3 clock’s time reference. However, for GPS satellites, both the PPP-B2b and GBM clock offset are determined against the L1/L2 IF combination signal; hence it does not need to be considered. Moreover, PPP-B2b and GBM products take the BDT and GPST as the reference, respectively. Thus, the time difference of 14 s between them should be eliminated.

2.2. Algorithms of B2b-RTPPP

The observation equations of the raw pseudorange P_i and raw carrier phase L_i at i th frequency are expressed as follows [27,28]:

$$P_i = \rho + c(dt_r - dt^s) + T + \gamma_i I_1 + c(d_{r,i} - d_i^s) + \varepsilon_i \quad (5)$$

$$L_i = \rho + c(dt_r - dt^s) + T - \gamma_i \cdot I_1 + \lambda_i (b_{r,i} - b_i^s + N_i) + \zeta_i \quad (6)$$

where the symbols r and s denote the receiver and satellite, respectively; ρ denotes the distance from the satellite to the receiver (in meters); dt_r and dt^s represent the receiver and satellite clock error (in seconds), respectively; T denotes the tropospheric wet delay (meters); $\gamma_i = f_1^2 / f_i^2$ is the frequency amplification factor; I_1 is the first-order ionospheric delay (in meters); d_r and b_r are the frequency-dependent pseudorange and carrier phase hardware delay at the receiver end, respectively; d^s and b^s denote pseudorange and carrier phase hardware delay at the satellite end, respectively; λ_i is the wavelength on f_i (meters); N_i is the float ambiguity (cycle); and ε_i and ζ_i indicate the unmodeled noises (meters). Note that the phase windup effect, tidal effect, relativistic effect, and satellite antenna APC were corrected. In this paper, 1, 3, 4, and 5 denote the B1I, B3I, L1, and L2 signals, respectively. The following notations are also used:

$$\left\{ \begin{array}{l} \alpha_{mn} = \frac{f_m^2}{f_m^2 - f_n^2} \\ \beta_{mn} = -\frac{f_n^2}{f_m^2 - f_n^2} \\ DCB_{mn}^s = d_m^s - d_n^s \\ DCB_{r,mn} = d_{r,m} - d_{r,n} \\ dt_{r,IF_{mn}} = dt_r + \alpha_{mn} d_{r,m} + \beta_{mn} d_{r,n} \\ dt_{IF_{mn}}^s = dt^s + \alpha_{mn} d_m^s + \beta_{mn} d_n^s \end{array} \right. , m, n = 1, 3, 4, 5, m \neq n \quad (7)$$

where α and β are frequency factors.

In this work, the B1I/B3I and L1/L2 combination observations were employed to realize the BDS-3 and GPS B2b-RTPPP time transfer, respectively. As mentioned above, the systematic bias of GPS satellites in PPP-B2b clock offset is the hardware delay of the L1/L2 IF combination, while that of BDS-3 satellites is the B3I. That is

$$\begin{cases} dt_{IF45}^s = dt^s + d_{IF45}^s \\ dt_{brd}^s = dt^s + d_3^s \end{cases} \quad (8)$$

By applying the PPP-B2b products, Equations (5) and (6) can be rewritten as [29]

$$\begin{cases} P_i = \rho + c(dt_r + d_{r,i} - dt_{brd}^s) - cDCB_{i3}^s + T + I_i + \varepsilon_1 \\ L_i = \rho + c(dt_r + d_{r,i} - dt_{brd}^s) + T - I_i + \lambda_i(b_{r,i} - b_i^s + N_i) + \zeta_i \end{cases}, i = 1, 3 \quad (9)$$

$$\begin{cases} P_j = \rho + c(dt_{r,IF45} - dt_{IF45}^s) + T + I_j + \varepsilon_j \\ L_j = \rho + c(dt_{r,IF45} - dt_{IF45}^s) + T - I_j + \lambda_j \bar{N}_j + \zeta_j \end{cases}, j = 4, 5 \quad (10)$$

with

$$\bar{N}_j = (N_j + b_{r,j} - b_j^s) - \frac{c}{\lambda_j}(d_{r,IF45} - d_{IF45}^s), j = 4, 5 \quad (11)$$

Based on Equations (9)–(11), the B1I/B3I and L1/L2 IF pseudorange function P_{IF13} and P_{IF45} and carrier phase function L_{IF13} and L_{IF45} can be expressed as

$$\begin{cases} P_{IF13} = \alpha_{13}P_1 + \beta_{13}P_3 = \rho + c(dt_{r,IF13} - dt_{brd}^s) - \alpha_{13}cDCB_{13}^s + T + \varepsilon_{13} \\ L_{IF13} = \alpha_{13}L_1 + \beta_{13}L_3 = \rho + c(dt_{r,IF13} - dt_{brd}^s) + T + \lambda_{13}\bar{N}_{13} + \zeta_{13} \end{cases} \quad (12)$$

$$\begin{cases} P_{IF45} = \alpha_{45}P_4 + \beta_{45}P_5 = \rho + c(dt_{r,IF45} - dt_{IF45}^s) + T + \varepsilon_{45} \\ L_{IF45} = \alpha_{45}L_4 + \beta_{45}L_5 = \rho + c(dt_{r,IF45} - dt_{IF45}^s) + T + \lambda_{45}\bar{N}_{45} + \zeta_{45} \end{cases} \quad (13)$$

$$\lambda_{13}\bar{N}_{13} = \alpha_{13}\lambda_1(b_{r,1} - b_1^s + N_1) + \beta_{13}\lambda_3(b_{r,3} - b_3^s + N_3) - c(dt_{r,IF13} + d_3^s) \quad (14)$$

$$\lambda_{45}\bar{N}_{45} = \alpha_{45}(N_4 + b_{r,4} + b_4^s) + \beta_{45}(N_5 + b_{r,5} + b_5^s) - c(d_{r,IF45} - d_{IF45}^s) \quad (15)$$

Based on Equations (12)–(15), the parameter vector to be estimated can be expressed as

$$\mathbf{X} = [\mathbf{x}, dt_{r,IFmn}, T, \lambda_{mn}\bar{N}_{mn}] \quad (16)$$

2.3. Time Transfer Model

Inter-station time transfer is the term used to describe time transfer. First, a receiver clock offset between the atomic clock's time and the reference time is obtained by the PPP engine. Second, the difference between the reference station clock offset and the other station clock offsets is calculated [30], which can be expressed as

$$\begin{aligned} dt &= \delta t_1 - \delta t_2 \\ &= (BDT_1 - t_{ref}) - (BDT_2 - t_{ref}) \\ &= BDT_1 - BDT_2 \end{aligned} \quad (17)$$

where δt indicates receiver clock of the local time of atomic clock (BDT) with respect to reference time (t_{ref}). Meanwhile, the hardware delay at the receiver end should be calibrated during GNSS data processing. Figure 1 shows the principle of the B2b-RTPPP.

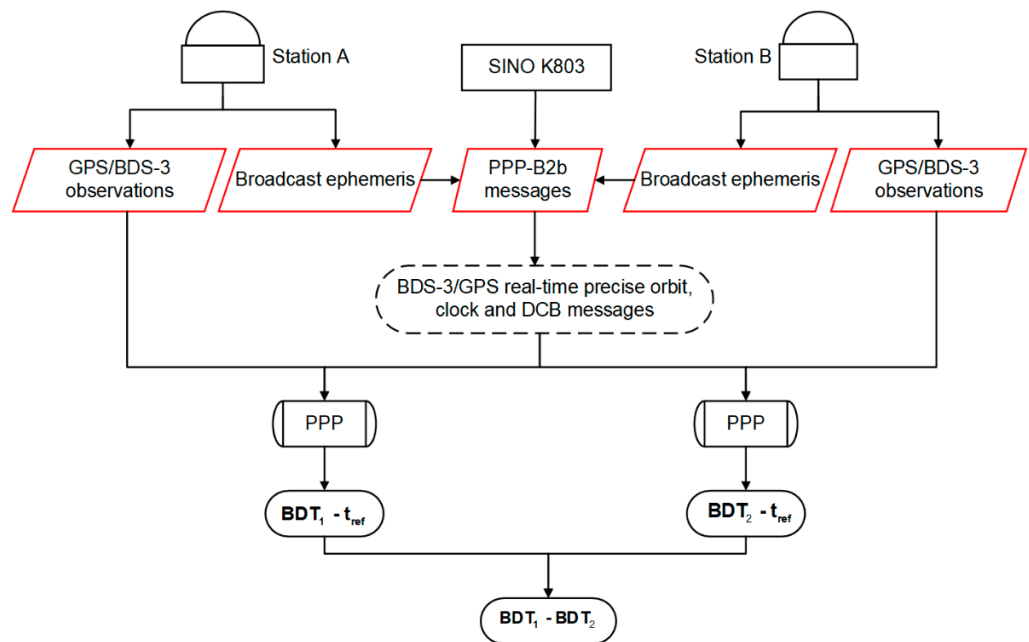


Figure 1. Principle of B2b-RTPPP.

3. Results

3.1. Experimental Data and Processing Strategies

The Multi-GNSS Experiment (MGEX) stations distributed across China and its surrounding areas provide real-time observations of navigation satellite systems. To assess the B2b-RTPPP time transfer performance with different constellations, we collected PPP-B2b messages using the SINO K803 kit, over a seven-day period from 2 April to 8 April, 2022 (DOY 92–98, 2022). Software developed based on the RTKLIB software package was used to decode the PPP-B2b products according to the ICD [22] and test PPP method. The GBM final products were downloaded from the GFZ. Figure 2 presents the location of five selected stations. Note that USUD station was taken as the central node, and four time links (MIZU-USUD, TLM2-USUD, JFNG-USUD, and LCK3-USUD) were designed.

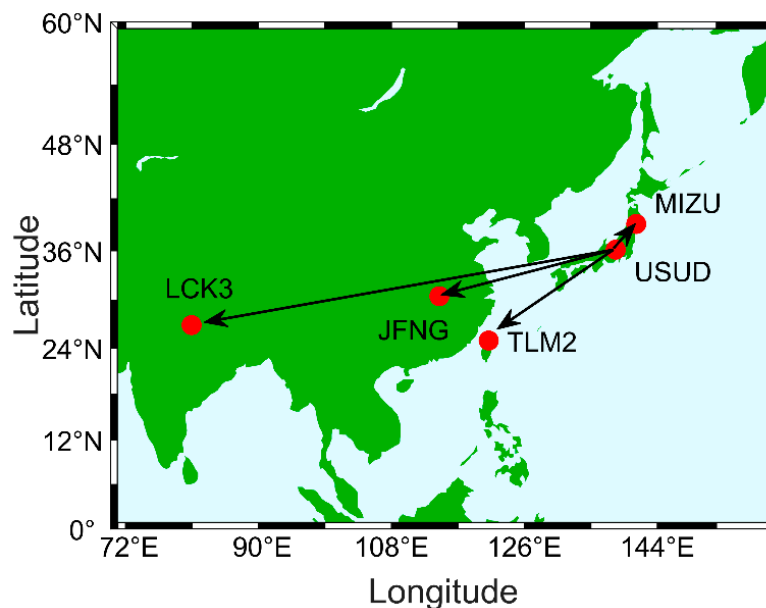


Figure 2. The location of selected stations used for B2b-RTPPP time transfer.

The stations were selected based on the following criteria: (1) they can simultaneously track B1I, B3I, L1, and L2 signals; (2) they are located in China and its surrounding areas; and (3) the receivers, if possible, are connected to high-performance on-board clocks. Table 2 provides information on the five stations. The B2b-RTPPP processing strategies are presented in Table 3.

Table 2. Information of selected stations.

Site	Receiver	Antenna	Clock	Distance from USUD (km)
USUD	SEPT POLARX5	AOAD/M_T	H-MASER	–
MIZU	SEPT POLARX5	SEPCHOKE_B3E6	CESIUM	413.3
TLM2	SEPT POLARX5TR	HEMA45	H-MASER	2060.2
JFNG	TRIMBLE ALLOY	TRM59800.00	–	2289.4
LCK3	TRIMBLE ALLOY	LEIAR25.R3	H-MASER	5303.9

Table 3. Processing strategies for the B2b-RTPPP.

Items	Methods
Observations	GPS: L1/L2; BDS-3: B1I/B3I
Sampling rate	30 s
Estimator	Kalman filter
Cut-off elevation	10°
Phase windup	Model corrected [31]
Tidal effect	Model corrected [32]
Relativistic effect	Model corrected [32]
Satellite orbit and clock offset	Broadcast ephemeris + PPP-B2b corrections
Satellite DCB	PPP-B2b DCB corrections
Receiver clock offset	Estimated as white noise
Receiver DCB	Estimated together with receiver clock offset
Satellite antenna APC	Fixed to the values from igs14.atx
	ZHD: Saastamoinen model [33]
Troposphere	ZWD: random walk estimation + GMF [34] mapping function
Phase ambiguities	Float

3.2. Quality Evaluation of PPP-B2b Corrections

The quality of the PPP-B2b orbit, clock offset, and DCB products was evaluated in this section. Then, the performance of B2b-RTPPP time transfer was analyzed. With the GBM final product as the reference, the PPP-B2b orbit and clock offset products' quality were assessed. In addition, the quality of PPP-B2b DCB was compared with that of the CAS DCB products. At present, both PPP-B2b and CNES RTS can provide real-time correction messages for BDS-3 (except C31) and GPS. The B2b-RTPPP time transfer performance is investigated employing the G, C, and GC observations. Note that due to space limitations, we only evaluated the PPP-B2b corrections for a specific time period. However, this will not have a limiting significance for the assessment of PPP-B2b product quality. Many works in the literature have evaluated the quality of PPP-B2b products [25,26,35,36].

3.2.1. PPP-B2b Orbit Corrections

The average root mean square error (RMSE) was employed to indicate the accuracy of the orbits. Figures 3–6 show the RMSEs of the PPP-B2b and CNES orbits in the R/A/C directions during the test period. The GBM final orbit product was used as the reference. The four figures show that the RMSEs of the CNES orbits are lower than those of the PPP-B2b orbits for both BDS-3 and GPS satellites, which is attributed to the fact that products from CNES are heavily reliant on global tracking stations, whereas those from PPP-B2b are primarily reliant on tracking stations in China [37]. As shown in Figures 4 and 6, GPS satellites have smaller RMSEs for CNES real-time orbits in the R/A/C directions

compared with those of the BDS-3 satellites. The RMSEs of GPS satellite orbits are within 0.10 m, and those of BDS-3 satellite orbits are within 0.30 m. Note that the CNES orbit has nearly the same accuracy in the three directions for GPS satellites. However, as shown in Figures 3 and 5, for the PPP-B2b orbit products, the RMSEs of the BDS-3 satellite orbits in the R/A/C directions perform better than those of the GPS satellite orbits, especially in the A component, which potentially benefits from the implementation of inter-satellite link (ISL) technology [35]. Because ISL can effectively improve the orbit determination, which can further provide a more accurate satellite position, especially in the A direction. Furthermore, we can see that the R direction has a minimum RMSE, while the RMSEs in the A and C directions are large, approximately two to four times that in the R direction. Therefore, the orbit error is primarily coming from the A component, which has the greatest impact on the orbit accuracy. Note that the C31, C38, C39, C40, G05, G11, G14, G23, G28, and G32 satellites were excluded from the comparison because the information of these satellites (except C38, C39, and C40) were not included in PPP-B2b products during the test period. Additionally, the quality of the orbit and clock offset for IGSO satellites (C38, C39, and C40) was poorer than that for MEO satellites [25].

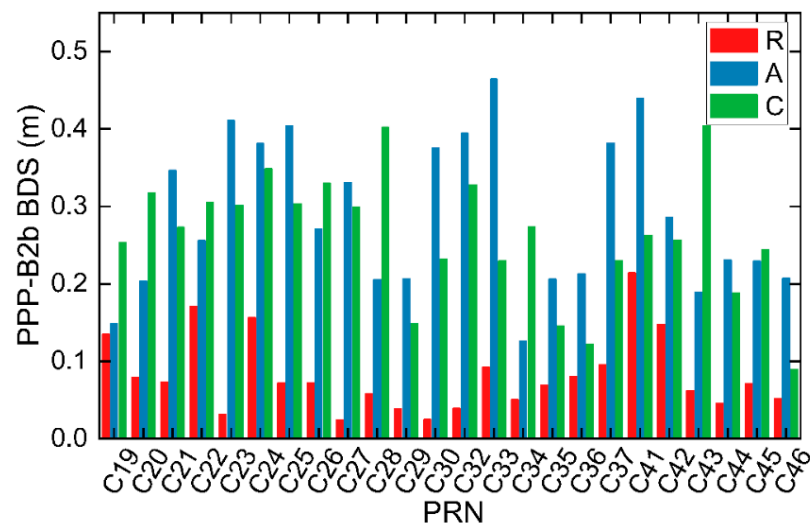


Figure 3. RMSEs of the PPP-B2b orbits for BDS-3 satellites.

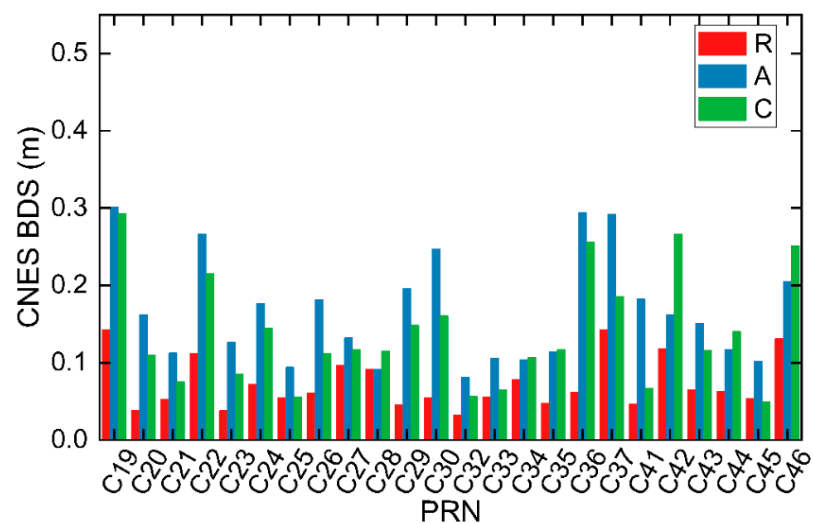


Figure 4. RMSEs of the CNES orbits for BDS-3 satellites.

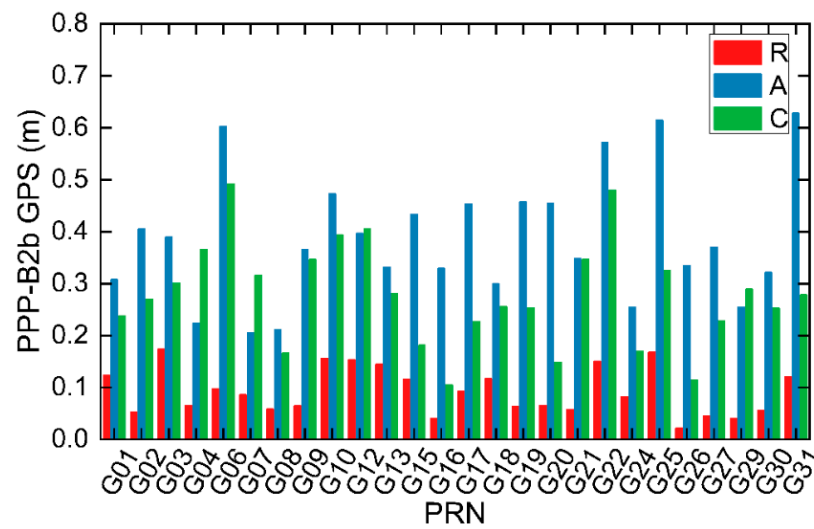


Figure 5. RMSEs of the PPP-B2b orbits for GPS satellites.

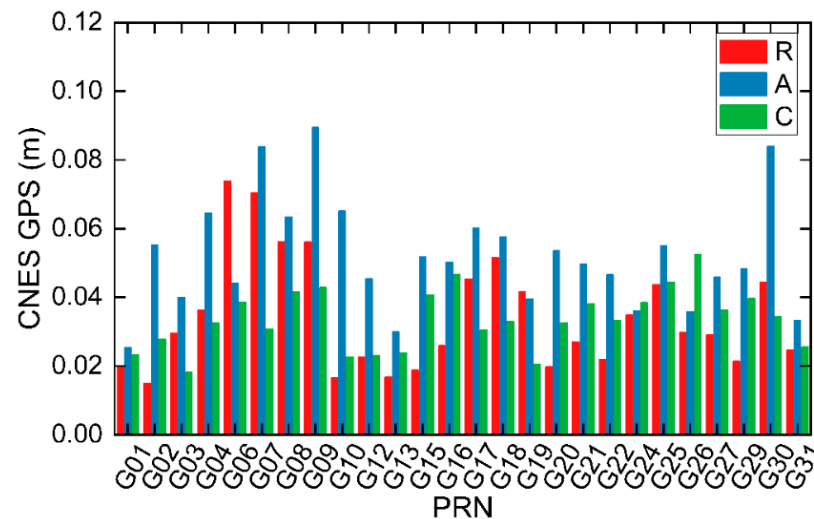


Figure 6. RMSEs of the CNES orbits for GPS satellites.

To further evaluate the precision of the PPP-B2b and CNES orbits, their average RMSEs were calculated, as presented in Table 4. For the BDS-3, the RMSEs are 0.082, 0.288, and 0.262 m in the R/A/C directions for the PPP-B2b real-time orbit, and 0.073, 0.166, and 0.138 m for the CNES real-time orbit. For the GPS, the RMSEs are 0.093, 0.386, and 0.278 m in the R/A/C directions for the PPP-B2b real-time orbit, and 0.034, 0.052, and 0.034 m for the CNES real-time orbit. Furthermore, the accuracy of the PPP-B2b orbit in the R direction is within 0.1 m, which is slightly lower than that of the CNES real-time orbit.

Table 4. Average RMSEs of BDS-3 and GPS orbits in the RAC directions (in meters).

Constellation	Service	R	A	C
BDS-3	PPP-B2b	0.082	0.288	0.262
	CNES	0.073	0.166	0.138
GPS	PPP-B2b	0.093	0.386	0.278
	CNES	0.034	0.052	0.034

3.2.2. PPP-B2b Clock Offset Corrections

The GBM final clock product was used as a benchmark to assess the quality of PPP-B2b and CNES clock offsets. It is worth noting that the clock offset of the broadcast ephemeris

and GBM final products could not be directly compared. Typically, a double-difference approach is adopted to assess the quality of the real-time clock product [38]. First, the difference between the real-time satellite clock offset and the satellite clock offset calculated by the GBM is required, which can be expressed as

$$\Delta dt^s = dt_{real-time}^s - dt_{GBM}^s \quad (18)$$

where the $dt_{real-time}^s$ is the satellite clock offset of the PPP-B2b or CNES; the dt_{GBM}^s is the satellite clock offset obtained by the GBM.

As the GNSS-specific timescales datum from different analysis centers and the frequency reference are different for the two products [39], there is a systematic bias in the difference. The double-difference method is used to eliminate the systematic bias:

$$\nabla \Delta dt^s = \Delta dt^s - \frac{1}{m} \sum_{i=0}^m \Delta dt^i \quad (19)$$

where $\nabla \Delta dt^s$ is the double-difference sequence and m is the available satellite number at each epoch.

Owing to the above biases, the standard deviation (GNSS) was used to assess the accuracy of the PPP-B2b clock offset products. Figures 7 and 8 show the average STD values of GPS and BDS-3 clock offset errors recovered from PPP-B2b and CNES over a seven-day period in the dataset. For the BDS-3 constellation, the average STDs of PPP-B2b and CNES are 0.10 ns and 0.17 ns, respectively. For the GPS constellation, the STD values of the PPP-B2b were comparable to that of the CNES, with average STDs of 0.11 ns and 0.09 ns, respectively. The average STD of BDS-3 is smaller than that of GPS for PPP-B2b, which also benefits from the ISL.

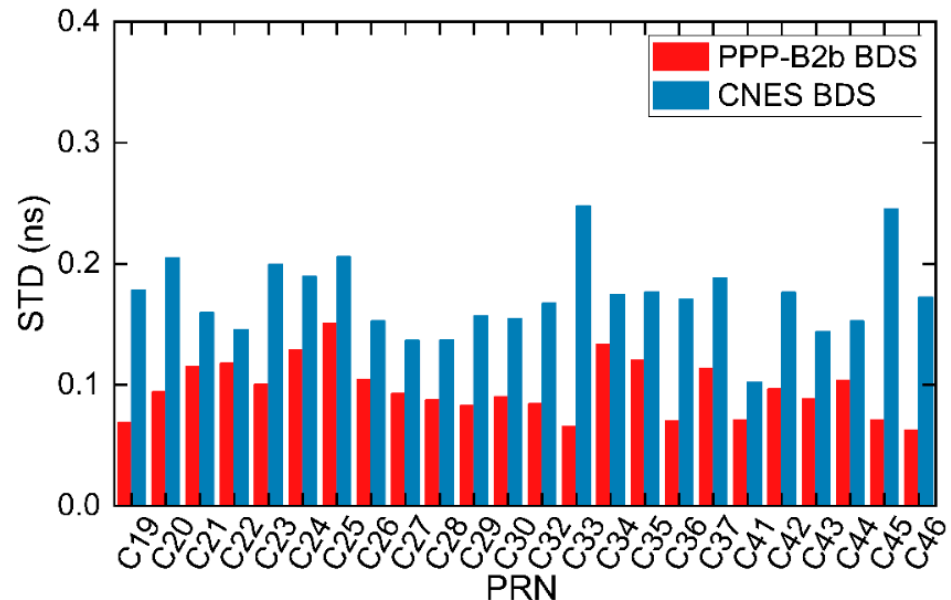


Figure 7. STDs of the PPP-B2b and CNES for BDS-3 satellite clock.

3.2.3. PPP-B2b DCB Corrections

Since three common DCB products were included in the PPP-B2b and CAS relative to the B3I signal (i.e., B1I-, B1Cp-, and B2ap-B3I DCB), only these three DCB products were evaluated. The PPP-B2b and CAS DCBs for each satellite are plotted in different colors in Figure 9. The PPP-B2b DCBs of B1I- and B1Cp-B3I showed good agreement with the CAS DCBs, while the B2ap-B3I DCB products indicated a strong systematic bias between PPP-B2b and CAS. We further summarized the biases of the PPP-B2b DCBs with respect to the CAS for each satellite, as shown in Figure 10. The B2ap-B3I DCB has the largest

difference, with an average value of 10.31 ns. However, the differences of B1I- and B1Cp-B3I DCB are almost the same, with average values of 0.91 ns and 1.36 ns, respectively. The STDs of biases are 0.68 ns, 0.54 ns, and 0.48 ns for B1I-, B1Cp-, and B2ap-B3I, respectively. Obviously, B1I-B3I DCB has the lowest stability. Therefore, the accuracy of the PPP-B2b DCB should be increased soon.

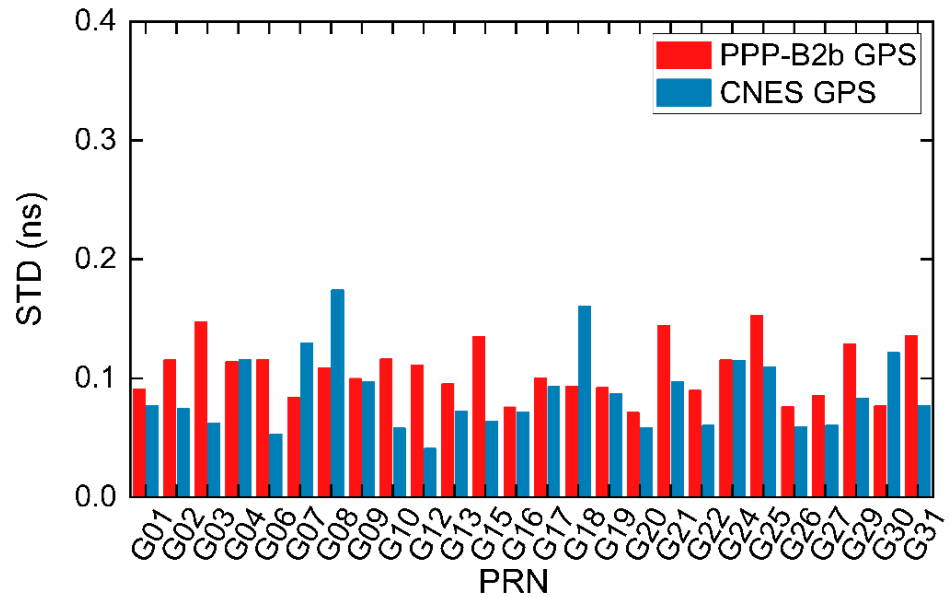


Figure 8. STDs of the PPP-B2b and CNES for GPS satellite clock.

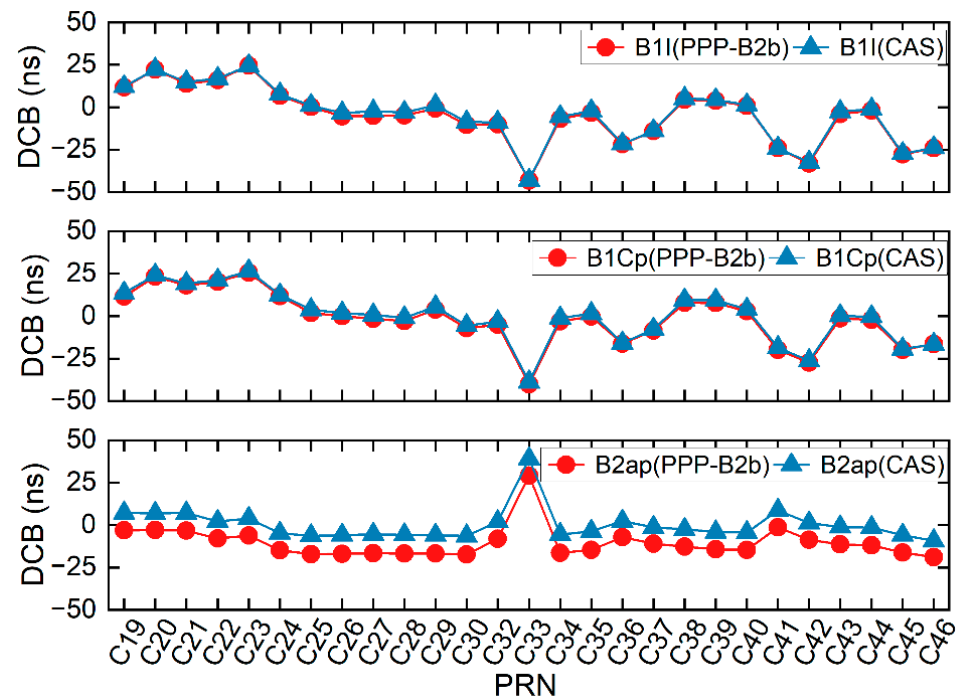


Figure 9. The DCB values of PPP-B2b and CAS for B1I-, B1Cp-, and B2ap-B3I.

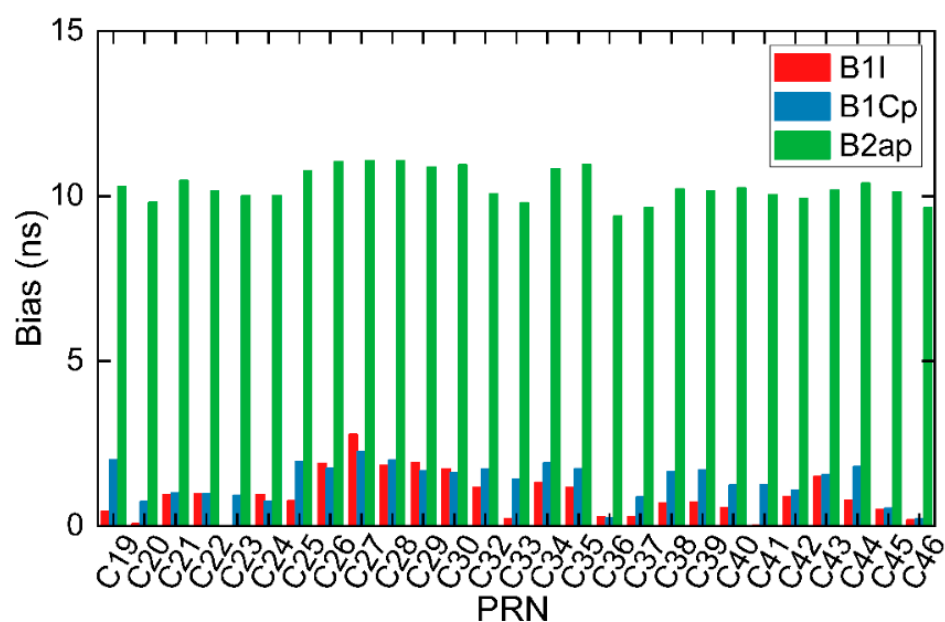


Figure 10. The DCB biases of the PPP-B2b with respect to CAS.

3.3. B2b-RTPPP Time Transfer with BDS-3/GPS Observations

With the observations of the B1I/B3I IF combination, the results of B2b-RTPPP time transfer using the post-processing PPP solution with GBM final product (GBM-PPP) were taken as a reference. As we concluded in Section 3.2.3, the quality of DCB products needs to be further improved in the near future. The performance of B2b-RTPPP time transfer with/without DCB corrections was investigated to analyze the contribution of DCB to B2b-RTPPP. The average STDs of the difference between B2b-RTPPP time link solutions and GBM-PPP time link solutions were calculated at each time link during the test period at a cut-off elevation angle of 10° , as shown in Figure 11. Note that the DCB of GPS was not provided by PPP-B2b. We have two key findings here. First, the STD values of the B2b-RTPPP solutions were all less than 1 ns. The STDs of the B2b-RTPPP solution without DCB correction were the largest (0.20–0.80 ns), approximately two to three times greater compared with those of the B2b-RTPPP solutions with DCB corrections (0.05–0.20 ns). It should be noted that the STD of the GC B2b-RTPPP solution was slightly lower than that of the C B2b-RTPPP solution. The G B2b-RTPPP solution had the greatest STD. The following three reasons can be used to explain above findings. (1) This is possibly due to the fact that the visible satellites of GPS are fewer than that of BDS-3. (2) For PPP-B2b, the quality of BDS-3 satellite's clock outperforms that of GPS, as shown by previous findings. (3) The pseudorange residual of B2b-RTPPP solutions without DCB is greater than that with DCB. Figure 12 presents the pseudorange residual on DOY 92. The DCB corrected pseudorange residual fluctuates around zero, while there is a systematic bias for the DCB noncorrected pseudorange residual. Thus, the DCB must be corrected in time transfer, otherwise, a part of the DCB will be absorbed by the station clock offset, reducing the B2b-RTPPP time transfer performance [40]. Second, in conjunction with Table 2 and Figure 11, it is found that the STD values of B2b-RTPPP solutions exhibit a strong correlation with the geographical distance of the time link. Interestingly, the STD values gradually increased as the distance of the time link increased. These relationships may be partially explained as follows. For the short baseline, most of the satellites tracked by two stations are the same. The satellite orbits and clock offsets have a similar effect on two stations that are close to each other, and the effect on the B2b-RTPPP solutions can be eliminated. For the long baseline, however, most of the satellites tracked by the two stations are not the same. The difference cannot be eliminated [41]. This resulted in differences in the B2b-RTPPP solutions for different time links at different distances.

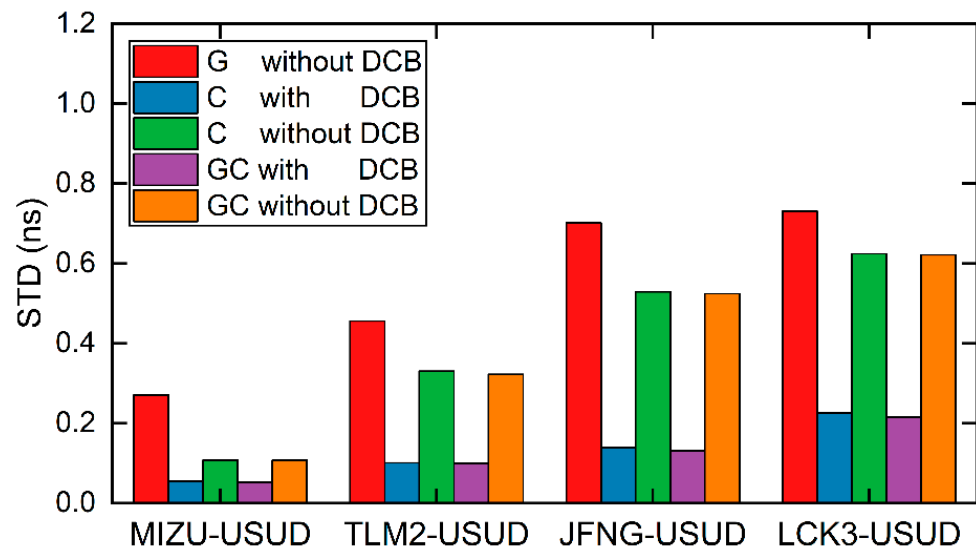


Figure 11. STD of difference between B2b-RTPPP solutions and GBM-PPP solutions.

The reductions of the C and GC B2b-RTPPP solutions with DCB compared with that without DCB at the STDs of the clock difference are illustrated in Table 5. For the C B2b-RTPPP, the reductions of STD ranged from 49.3% to 73.6%, with a mean reduction of 64%. The reductions of GC B2b-RTPPP were almost the same as that of GC B2b-RTPPP. Therefore, the DCB had a great impact on the time transfer, which validated our previous findings. In addition, compared with G B2b-RTPPP, the reductions of the C and GC B2b-RTPPP solutions with DCB ranged from 69.0–80.1% and 70.6–81.3%, with a mean reduction of 76.7% and 77.7%, respectively. For the B2b-RTPPP without DCB, STDs were reduced by at least 14.5%, and by a maximum of 60.1% for C B2b-RTPPP. STDs were reduced by at least 14.6%, and by a maximum of 60.4% for GC B2b-RTPPP. Thus, the C and GC B2b-RTPPP performed better than the G B2b-RTPPP.

Table 5. The reduction of C and GC B2b-RTPPP solutions with DCB compared to that without DCB at STD values for clock difference (%).

	MIZU-USUD	TLM2-USUD	JFNG-USUD	LCK3-USUD
BDS-3-only	49.3	69.4	73.6	63.7
GPS + BDS-3	50.9	69.5	75.0	65.5

Frequency stability is another indicator of the time transfer performance. It should be noted that the frequency stability analysis is affected by both the device under test and the reference device. Three-corner-hat (TCH) method can provide a better separation between the noise in the links and the noise in the station clocks. We first performed the frequency stability analysis for all the stations according to the literature [42] using the TCH and found that all the links except the TLM2-USUD link had a high percentage of noise in the time link due to the excessive noise of one of the stations. In this case, the frequency stability experiment is a failure. Therefore, we only evaluate the TLM2-USUD time link. In this paper, we define averaging time less than 1000 s as short-term and averaging time greater than 10,000 s as long-term.

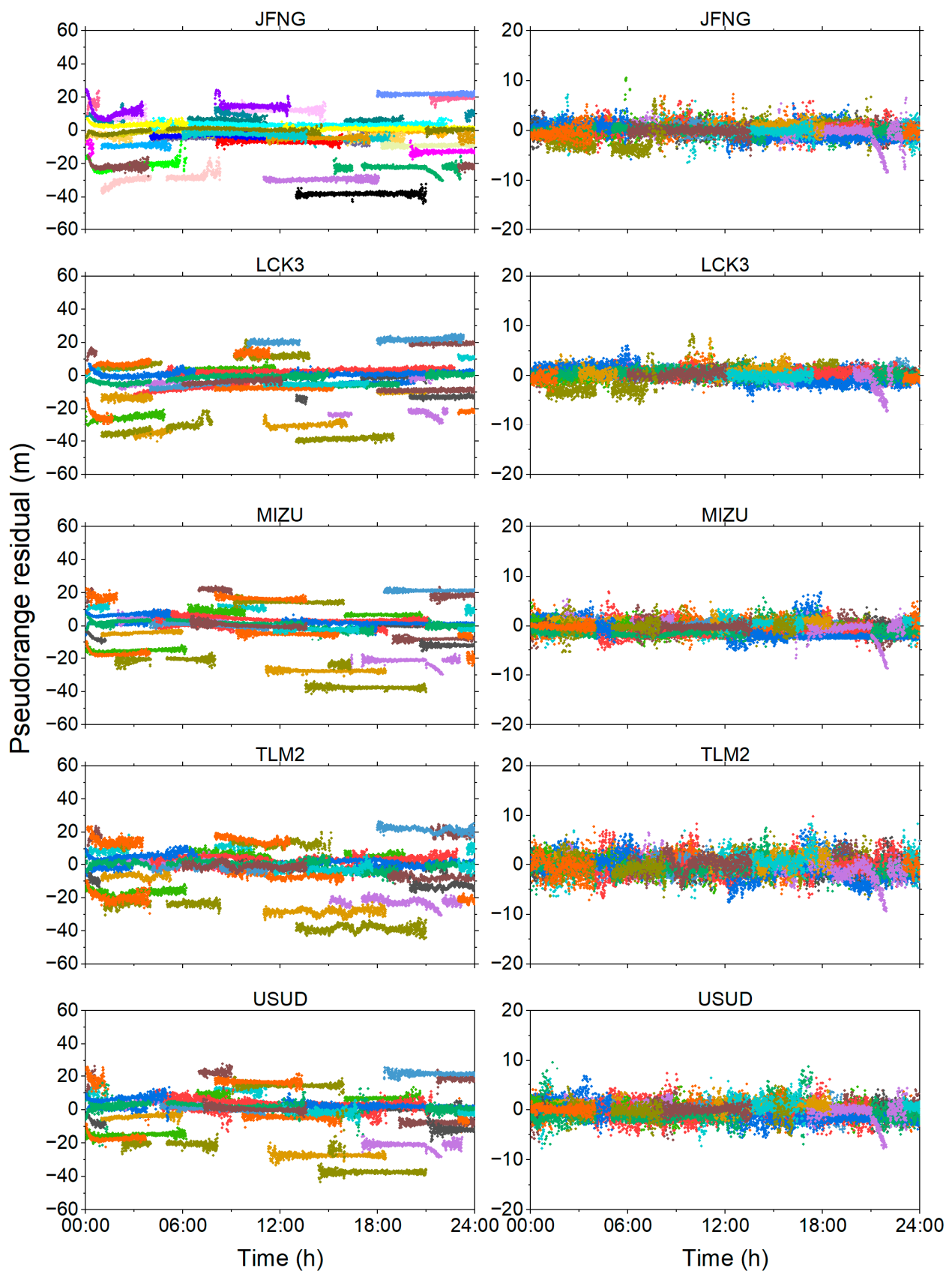


Figure 12. Pseudorange residual of B2b-RTPPP without (**left**) and with (**right**) DCB corrections. Each color represents a satellite.

Figure 13 shows the modified Allan deviation (MDEV) of the TLM2-USUD time link. For the five schemes, the G, C, and GC B2b-RTPPP solutions demonstrated a relatively high similarity at the same averaging time, while the G B2b-RTPPP solution had the poorest frequency stability in the long term. The MDEV of GC B2b-RTPPP solution with DCB performed better than the other solutions for most of the averaging time. In terms of short-term frequency stability, the MDEV of the G without DCB, C with DCB, C without DCB, GC with DCB, and GC without DCB are $(1.13 \times 10^{-13}, 4.06 \times 10^{-14}, 7.86 \times 10^{-14}, 3.62 \times 10^{-14},$ and $6.18 \times 10^{-14})$ at 960 s. In terms of long-term frequency stability for four time links, the MDEV of the G without DCB, C with DCB, C without DCB, GC with DCB, and GC without DCB are $(6.52 \times 10^{-15}, 1.49 \times 10^{-15}, 6.17 \times 10^{-15}, 1.40 \times 10^{-15},$ and $6.12 \times 10^{-15})$ at 122,880 s. These findings of frequency stability are similar to the STD values of B2b-RTPPP solutions. The enhancements of GPS satellites to BDS-3 PPP are limited the PPP-B2b corrections. As our previous evaluation of the PPP-B2b product concluded, the quality of the GPS satellites is inferior to that of the BDS-3 satellites. In addition, the frequency stability improved as the averaging time increased. It should be noted that compared with the MDEV without DCB correction, the MDEV with DCB correction was similar in the short-term, while the B2b-RTPPP solutions with DCB demonstrated better long-term MDEV. The main reason for the frequency stability without DCB correction is that the large pseudorange residuals without DCB correction led to additional errors absorbed by the receiver clock offset. The frequency stability of the B2b-RTPPP solutions without DCB was significantly poorer at the TLM2-USUD time link than that of the B2b-RTPPP solutions with DCB, which is analyzed below.

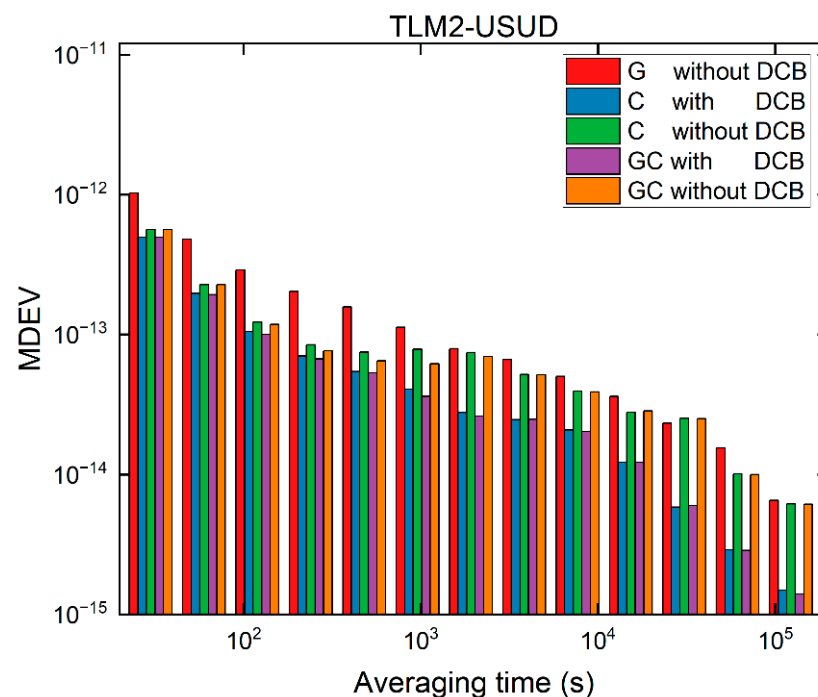


Figure 13. The TCH results for the TLM2-USUD time link.

To verify the previous findings, the number of satellites involved in B2b-RTPPP at a cut-off elevation angle of 10° for the TLM2 and USUD stations during the test period are shown in Figure 14. The average number of visible satellites is 7.8, 8.6, and 16.4 for the G, C, and GC at the TLM2 station; and 8.3, 8.6, and 16.9 for the G, C, and GC at the USUD station, respectively. In addition, there were relatively fewer GPS satellites at the TLM2 station; up to five satellites at some epochs, leading to the appearance of outliers and reconvergence [43], as shown in Figure 15, which presents the clock difference between the two station clock offsets. The uncorrected DCB solutions had a slower convergence rate, which reduced the B2b-RTPPP time transfer. This also decreased the frequency stability.

Note that a systematic bias was observed between the G and C B2b-RTPPP solutions, which was attributed to the different hardware delays absorbed by different IF combinations clock offset.

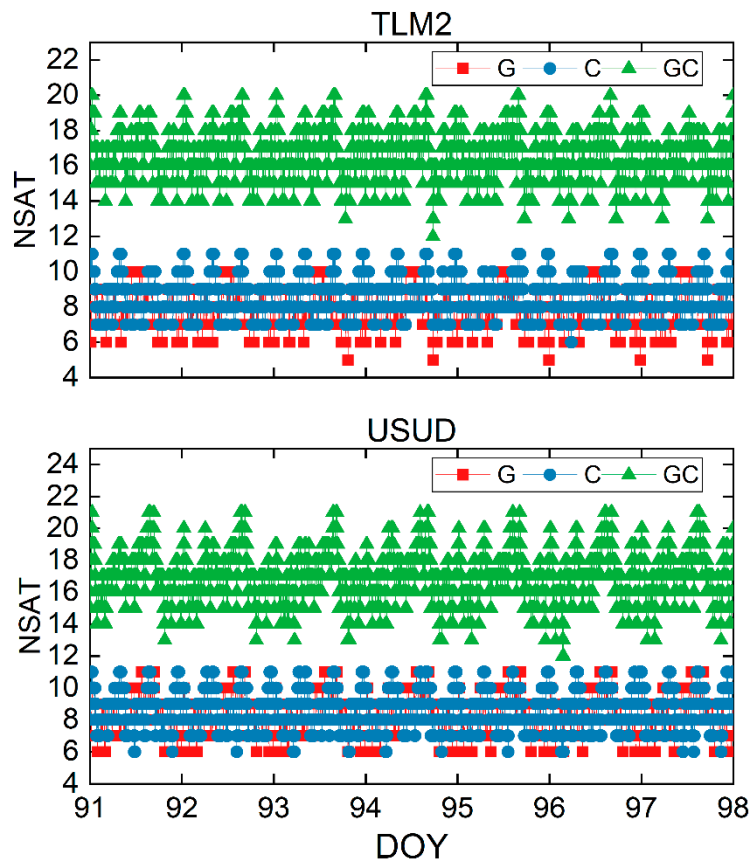


Figure 14. Number of visible satellites (NSAT) for TLM2 (top) and USUD (bottom) stations at a mask angle of 10°.

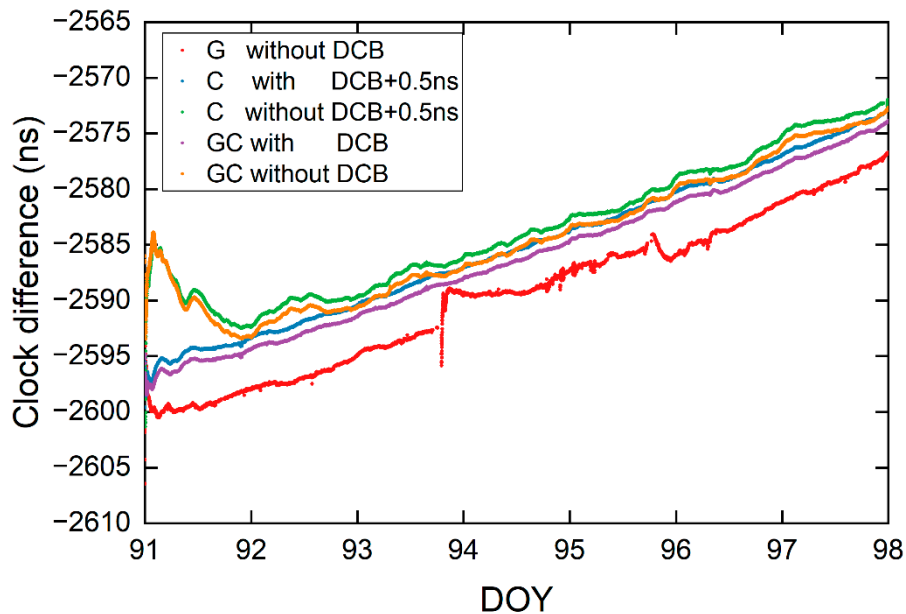


Figure 15. Clock difference of the B2b-RTPPP solutions for the TLM2-USUD time link.

3.4. B2b-RTPPP Time Transfer under Constrained Sky-View

As we know, the receiver may be blocked artificially or naturally, which means less sky-view. In this case, fewer satellites can be observed by the receiver. Additionally, the cut-off elevation angle is an important preset parameter of PPP. Since the atmospheric delay error and multipath error become larger as the angle decreases, the possibility of uncontrollable factors appearing on the signal propagation path is also higher, so a large cut-off elevation angle can weaken the influence of the above errors as much as possible [44,45]. Considering that the PPP-B2b performance in terms of elevation angle is unknown, we conducted a time transfer experiment at different cut-off elevation angles to analyze its effect on B2b-RTPPP. The cut-off elevation angle ranged from 10° to 40° , with a step of 10° . On the basis of previous findings, we only carried out GC B2b-RTPPP time transfer to avoid frequent outliers and re-convergence of time transfer because of the lack of trackable satellites.

Figure 16 displays the clock difference of the TLM2-USUD time link. The sequence of clock difference substantially overlaps at 10° , 20° , and 30° , while the fluctuation range is larger at 40° , which is mainly due to the poorer spatial geometric distribution of visible satellites. In addition, the PDOP values of TLM2 and USUD stations are shown in Figure 17. As we can see, the PDOP values increase gradually as the cut-off elevation angle rises. The average PDOPs are statistically 1.4, 1.8, 2.7, and 5.0 for the TLM2 station, and 1.3, 1.7, 2.7, and 4.8 for the USUD station at 10° , 20° , 30° , and 40° , respectively. The sequence of PDOP values for the TLM2 station has a larger fluctuation at a cut-off elevation angle of 40° . Therefore, B2b-RTPPP can obtain a relatively great time transfer solution at a lower cut-off elevation angle in theory.

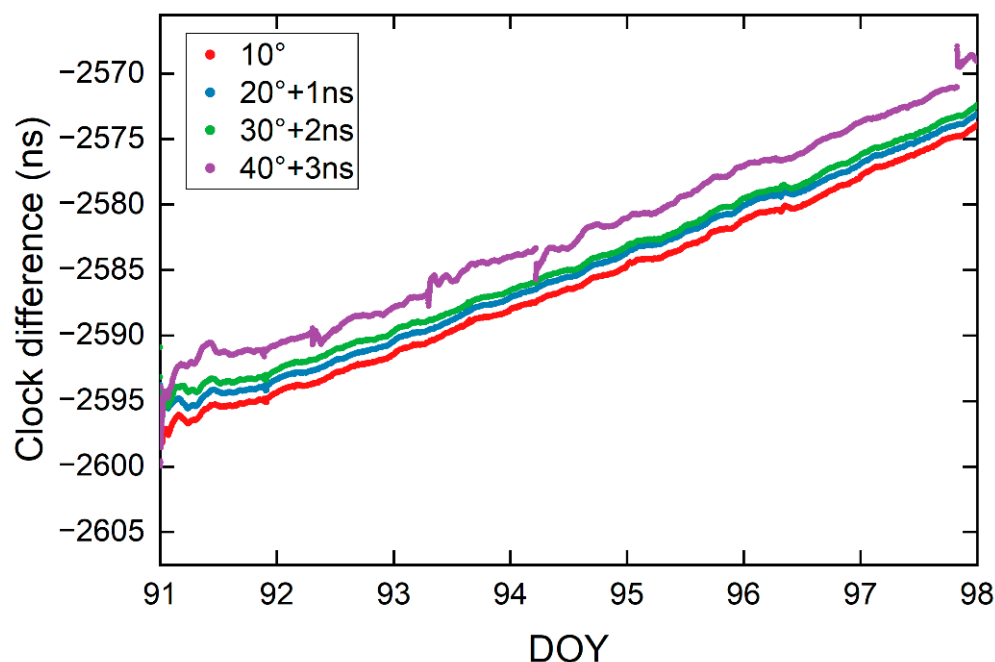


Figure 16. Clock difference of the TLM2-USUD time link.

To comprehensively investigate the performance of the B2b-RTPPP time transfer, the STDs of the difference between B2b-RTPPP solutions and GBM-PPP solutions are shown in Figure 18. The B2b-RTPPP time transfer performance decreased as the cut-off elevation angle increased. Moreover, the STD values of the clock difference were within 0.2 ns at the cut-off elevation angle from 10° to 30° , with no significant difference. However, the STD values present a significant increase at a mask angle of 40° , approximately two to four times greater than the STD values at a mask angle of 10° . It is worth noting that the STD values were all within 1 ns with different B2b-RTPPP solutions. Furthermore,

Table 6 shows the improvement of the B2b-RTPPP solution with the mask angles of 10° , 20° , and 30° compared with the B2b-RTPPP solution with the angle of 40° at the STDs for the clock difference. Compared with the B2b-RTPPP solution at the mask angle of 40° , the B2b-RTPPP solutions at the mask angles of 10° , 20° , and 30° improved by 71.9–80.6%, 64.1–78.1%, and 58.3–74.5%, with a mean reduction of 76.1%, 70.8%, and 67.8%, respectively. Overall, the STDs of the B2b-RTPPP solution for all time links varied within an acceptable range for the B2b-RTPPP time transfer.

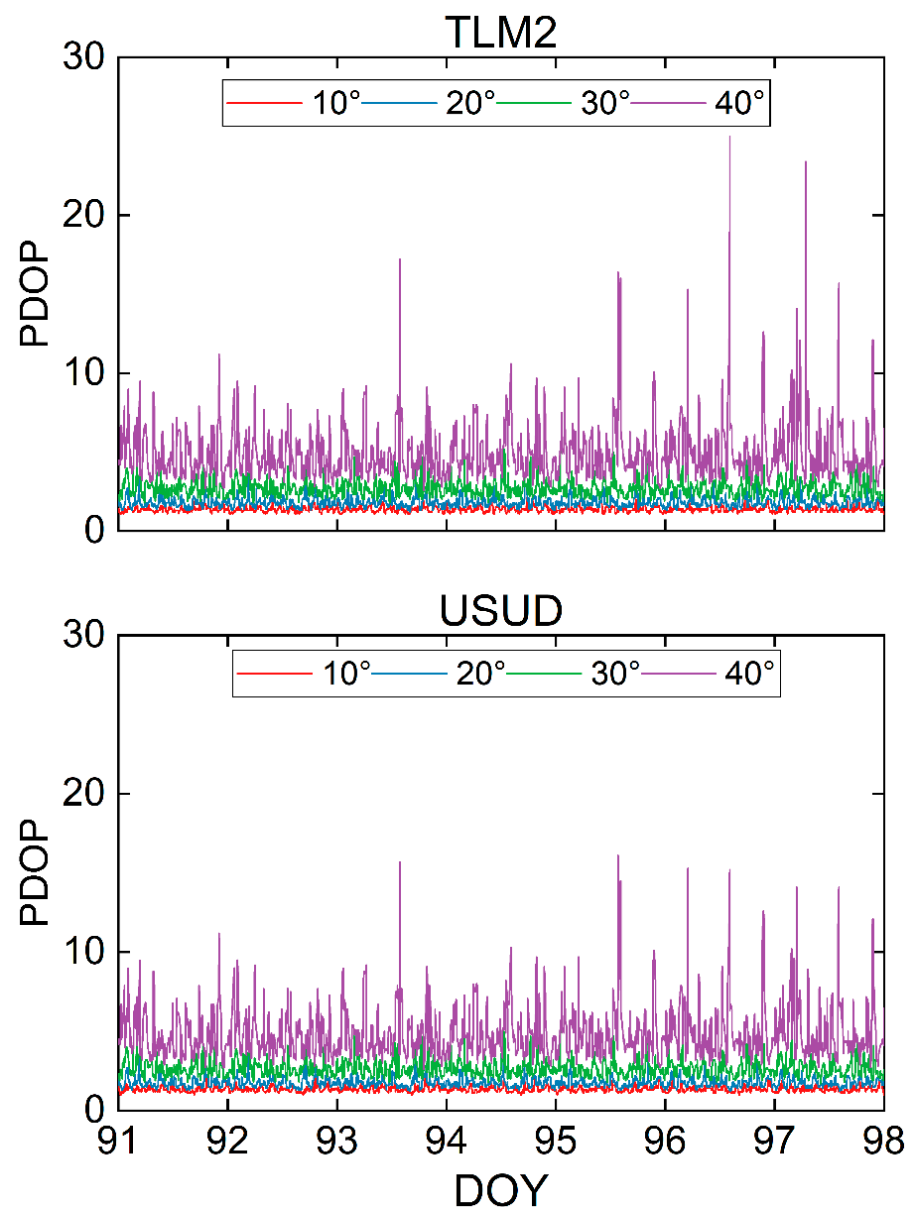


Figure 17. PDOP values of the TLM2 (top) and USUD (bottom) station.

Figure 19 depicts the MDEV of the TLM2-USUD time link. No significant difference in the MDEV was observed in the short term. The MDEV of 10° , 20° , 30° , and 40° are 2.33×10^{-14} , 2.14×10^{-14} , 2.39×10^{-14} , and 2.35×10^{-14} at 960s. The mean MDEVs of 10° , 20° , 30° , and 40° are 1.07×10^{-15} , 1.03×10^{-15} , 1.35×10^{-15} , and 1.78×10^{-15} at 122,880 s. As the cut-off elevation angle increased, the long-term frequency stability decreased. In addition, the frequency stability of the TLM2-USUD time link outperformed those of other time links at the same averaging time. A possible explanation for this may be that the

TLM2 and USUD stations are connected to atomic clocks with higher precision, which have lower noise level.

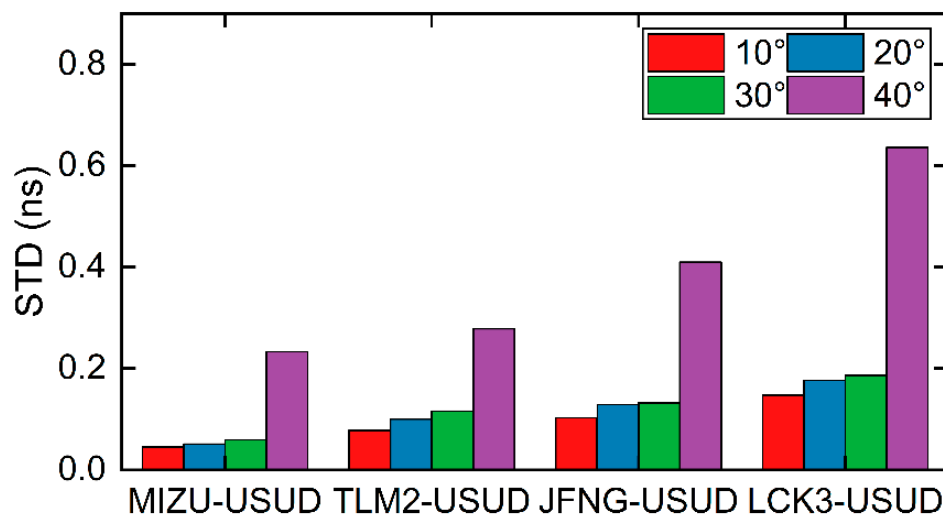


Figure 18. STDs of difference between B2b-RTPPP and GBM-PPP solutions.

Table 6. The improvement of the B2b-RTPPP solution with mask angles of 10°, 20°, and 30° compared with the B2b-RTPPP solution with the angle of 40° at the STDs for the clock difference (%).

	MIZU-USUD	TLM2-USUD	JFNG-USUD	LCK3-USUD
10°	80.6	71.9	75.0	76.8
20°	78.1	64.1	68.5	72.3
30°	74.5	58.3	67.8	70.6

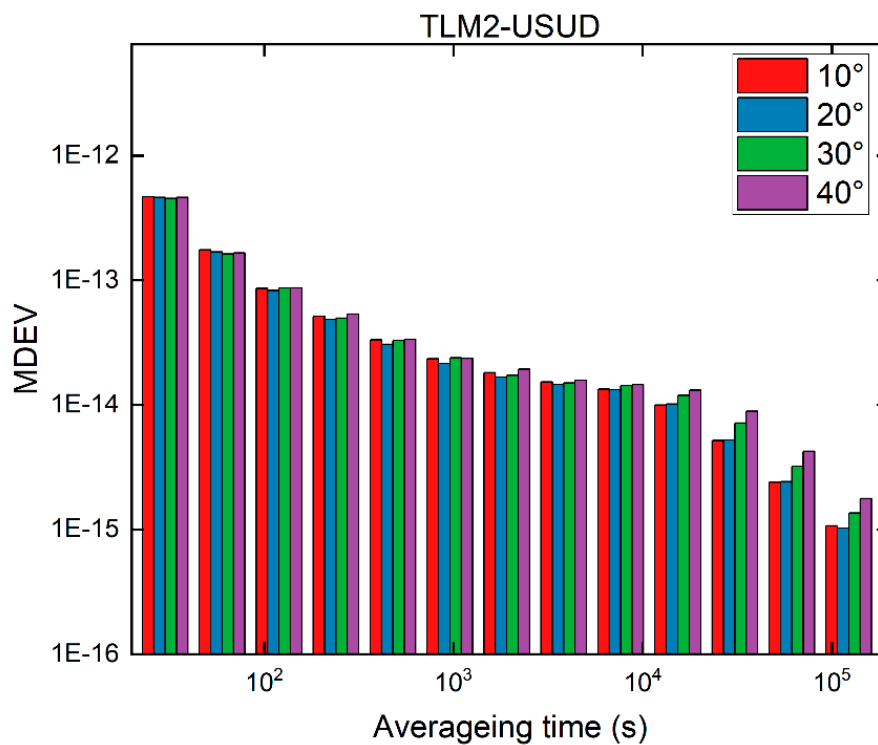


Figure 19. The TCH results for TLM2-USUD time link.

4. Discussion

According to the results, the PPP-B2b orbit and clock offset are in good agreement with the GBM product. Compared with the CNES orbit, the PPP-B2b orbital accuracy is poor, which may be caused by the regional monitoring stations of PPP-B2b. For PPP-B2b, the application of ISL makes the orbit and clock accuracy of BDS-3 higher than GPS. In addition, according to the results, PPP-B2b DCB and CAS DCB also have good consistency, while B1I-B3I DCB has a relatively large deviation. Thus, the accuracy of PPP-B2b DCB needs to be further improved.

The B2b-RTPPP time transfer accuracy has a strong correlation with the baseline length. The longer the baseline length, the worse the time transfer accuracy. This is mainly related to the satellite orbit errors and clock errors observed by the two stations. With a short baseline, more common satellites can be observed, and the effects of orbit errors and clock errors on time transfer can be eliminated. For long baselines, these errors cannot be eliminated.

DCB has a great influence on time transfer. After DCB is corrected, the time transfer accuracy of B2b-RTPPP is improved significantly. DCB has a certain influence on frequency stability: the pseudorange residuals of the uncorrected DCB are greater causing the receiver to absorb part of the error, which in turn leads to a decrease in frequency stability.

The cut-off elevation angle also has a great influence on the time transfer. At a large cut-off elevation angle, the time transfer performance of B2b-RTPPP will be reduced. When the angle reaches 40° , the B2b-RTPPP time transfer is not continuous, and the B2b-RTPPP time transfer is not discontinued, and frequent interruptions and reconvergence occur due to the sharp decrease in visible satellites.

5. Conclusions

The BDS-3 began providing RTS to users in the Asia-Pacific region in 2020 using the PPP-B2b signal, offering promising opportunities for real-time PPP. In our contribution, the quality of PPP-B2b products was first evaluated with reference to GBM final products. Furthermore, the B2b-RTPPP time transfer performance was assessed using observation data from five selected stations over a seven-day period (DOY 92–98 in 2022). The conclusions are as follows.

First, compared with the PPP-B2b GPS orbit, the PPP-B2b BDS-3 orbit has higher accuracy. The accuracy of the BDS-3 and GPS orbit in the R direction is centimeter-level. The accuracy of the BDS-3 orbit was better than that of the GPS orbit in the A direction owing to the additional ISL observations. Due to the limitations of the few regional observation stations, the PPP-B2b orbit accuracy performs worse than the CNES orbit for both GPS and BDS-3 satellites. For the BDS-3 satellites, the accuracy of the PPP-B2b clock offset outperforms that of the CNES. For the GPS satellites, the PPP-B2b clock's accuracy was lower than the CNES clock's. In terms of the PPP-B2b DCB, the biases of the PPP-B2b DCB are almost the same for all satellites with the CAS DCB as a reference. The average biases of the PPP-B2b DCB for B1I-, B1Cp-, and B2ap-B3I are 0.91 ns, 1.36 ns, and 10.31 ns, with STDs of 0.68 ns, 0.54 ns, and 0.48 ns, respectively.

Second, B2b-RTPPP time transfer experiments using G, C, and GC observations were carried out. The accuracy of G, C, and GC B2b-RTPPP time transfer is sub-nanosecond level. The GC B2b-RTPPP solution exhibited the best performance, while the G B2b-RTPPP solution had the worst performance due to fewer satellites and the DCB corrections. Compared with the accuracy of uncorrected DCB solutions, the accuracy with DCB correction was improved by 64%. For the STD with DCB correction, the mean reductions in the STD are approximately 76.7% and 77.7%, respectively, compared with the G B2b-RTPPP solution. In addition, the performance of the B2b-RTPPP time transfer may suffer as a result of the increase in the baseline of the time link. Time transfer experiments at different cut-off elevation angles showed that time transfer performance decreased as the cut-off elevation angle increased, especially at large angles. To sum up, excitingly, a subnanosecond-level accuracy can be achieved by the B2b-RTPPP time transfer.

Finally, the B1C/B2a IF combination has the smallest noise amplification factor among all dual-frequency combinations, which enables better PPP performance. Our further work will be conducted to investigate the B2b-RTPPP time transfer performance using observations of B1C/B2a IF combination. Considering the quality of the PPP-B2b DCB, analyzing the effect of the DCB on B2b-RTPPP time transfer will also be a focus in future work.

Author Contributions: J.T.: methodology, software, investigation, writing—original draft preparation. D.L.: conceptualization, methodology, validation, data curation, writing—review and editing. F.Z.: validation, resources, supervision, project administration. Y.G.: formal analysis, project administration, funding acquisition. R.Z.: visualization, formal analysis. All authors have read and agreed to the published version of the manuscript.

Funding: The research was funded by National Natural Science Foundation of China (No. 42204039).

Data Availability Statement: The datasets in this study are available by contacting the corresponding author.

Acknowledgments: We appreciate MGEX, GFZ, CAS, and CSNO for providing experimental data.

Conflicts of Interest: The authors declare no conflict of interest.

References

- Zumberge, J.F.; Heftin, M.B.; Jefferson, D.C.; Watkins, M.M.; Webb, F.H. Precise Point Positioning for the Efficient and Robust Analysis of GPS Data from Large Networks. *J. Geophys. Res. Solid Earth* **1997**, *102*, 5005–5017. [[CrossRef](#)]
- Kouba, J.; Héroux, P. Precise Point Positioning Using IGS Orbit and Clock Products. *GPS Solut.* **2001**, *5*, 12–28. [[CrossRef](#)]
- Ray, J.; Senior, K. Geodetic Techniques for Time and Frequency Comparisons Using GPS Phase and Code Measurements. *Metrologia* **2005**, *42*, 215–232. [[CrossRef](#)]
- Petit, G. The TAIPPP Pilot Experiment. In Proceedings of the 2009 IEEE International Frequency Control Symposium Joint with the 22nd European Frequency and Time Forum, Besancon, France, 20–24 April 2009; pp. 116–119.
- Arias, E.F.; Panfilo, G.; Petit, G. Timescales at the BIPM. *Metrologia* **2011**, *48*, S145–S153. [[CrossRef](#)]
- Jin, S.; Komjathy, A. GNSS Reflectometry and Remote Sensing: New Objectives and Results. *Adv. Space Res.* **2010**, *46*, 111–117. [[CrossRef](#)]
- Du, Y.; Wang, J.; Rizos, C.; El-Mowafy, A. Vulnerabilities and Integrity of Precise Point Positioning for Intelligent Transport Systems: Overview and Analysis. *Satell. Navig.* **2021**, *2*, 3. [[CrossRef](#)]
- Liu, T.; Zhang, B.; Yuan, Y.; Zhang, X. On the Application of the Raw-Observation-Based PPP to Global Ionosphere VTEC Modeling: An Advantage Demonstration in the Multi-Frequency and Multi-GNSS Context. *J. Geod.* **2020**, *94*, 1. [[CrossRef](#)]
- Liu, W.; Chen, S.; Ge, J.; Yuan, H.; Gong, C. Research on Nanosecond Time Synchronization Technology for 5G Base Station Based on GNSS Neighborhood Similarity. *J. Commun.* **2020**, *41*, 180–190. [[CrossRef](#)]
- Liu, T.; Zhang, B.; Yuan, Y.; Li, M. Real-Time Precise Point Positioning (RTPPP) with Raw Observations and Its Application in Real-Time Regional Ionospheric VTEC Modeling. *J. Geod.* **2018**, *92*, 1267–1283. [[CrossRef](#)]
- Petit, G.; Jiang, Z. GPS All in View Time Transfer for TAI Computation. *Metrologia* **2008**, *42*, 35–42. [[CrossRef](#)]
- Elsobeiey, M.; Al-Harbi, S. Performance of Real-Time Precise Point Positioning Using IGS Real-Time Service. *GPS Solut.* **2016**, *20*, 565–571. [[CrossRef](#)]
- Ge, Y.; Qin, W.; Su, K.; Yang, X.; Ouyang, M.; Zhou, F.; Zhao, X. A New Approach to Real-Time Precise Point-Positioning Timing with International GNSS Service Real-Time Service Products. *Meas. Sci. Technol.* **2019**, *30*, 125104. [[CrossRef](#)]
- Mimura, D.; Miyatake, K.; Kubo, Y.; Sugimoto, S. Positioning Accuracy of Single Frequency GNSS PPP by CLAS Comparing with MADOCA Products. In Proceedings of the ISCIE International Symposium on Stochastic Systems Theory and its Applications, Fukushima, Japan, 1–2 November 2019; pp. 43–48. [[CrossRef](#)]
- Rovira-Garcia, A.; Timoté, C.C.; Juan, J.M.; Sanz, J.; González-Casado, G.; Fernández-Hernández, I.; Orus-Perez, R.; Blonski, D. Ionospheric Corrections Tailored to the Galileo High Accuracy Service. *J. Geod.* **2021**, *95*, 130. [[CrossRef](#)]
- Shi, C.; Wu, X.; Zheng, F.; Wang, X.; Wang, J. Modeling of BDS-2/BDS-3 Single-Frequency PPP with B1I and B1C Signals and Positioning Performance Analysis. *Measurement* **2021**, *178*, 109355. [[CrossRef](#)]
- Qin, W.; Ge, Y.; Wei, P.; Dai, P.; Yang, X. Assessment of the BDS-3 on-Board Clocks and Their Impact on the PPP Time Transfer Performance. *Measurement* **2020**, *153*, 107356. [[CrossRef](#)]
- Yang, Y.; Ding, Q.; Gao, W.; Li, J.; Xu, Y.; Sun, B. Principle and Performance of BDSBAS and PPP-B2b of BDS-3. *Satell. Navig.* **2022**, *3*, 5. [[CrossRef](#)]
- Zhang, W.; Lou, Y.; Song, W.; Sun, W.; Zou, X.; Gong, X. Initial Assessment of BDS-3 Precise Point Positioning Service on GEO B2b Signal. *Adv. Space Res.* **2022**, *69*, 690–700. [[CrossRef](#)]
- Chen, J.; Wang, A.; Zhang, Y.; Zhou, J.; Yu, C. BDS Satellite-Based Augmentation Service Correction Parameters and Performance Assessment. *Remote Sens.* **2020**, *12*, 766. [[CrossRef](#)]

21. Yang, Y.; Mao, Y.; Sun, B. Basic Performance and Future Developments of BeiDou Global Navigation Satellite System. *Satell. Navig.* **2020**, *1*, 1. [[CrossRef](#)]
22. CSNO BeiDou Navigation Satellite System Signal in Space Interface Control Document Precise Point Positioning Service Signal PPP-B2b, Version 1.0. Available online: <http://www.Beidou.Gov.Cn/Xt/Gfxz/202008/P020200803362062482940.Pdf> (accessed on 4 March 2022).
23. Lu, X.; Chen, L.; Shen, N.; Wang, L.; Jiao, Z.; Chen, R. Decoding PPP Corrections from BDS B2b Signals Using a Software-Defined Receiver: An Initial Performance Evaluation. *IEEE Sens. J.* **2021**, *21*, 7871–7883. [[CrossRef](#)]
24. Yang, H.; Ji, S.; Weng, D.; Wang, Z.; He, K.; Chen, W. Assessment of the Feasibility of PPP-B2b Service for Real-Time Coseismic Displacement Retrieval. *Remote Sens.* **2021**, *13*, 5011. [[CrossRef](#)]
25. Xu, Y.; Yang, Y.; Li, J. Performance Evaluation of BDS-3 PPP-B2b Precise Point Positioning Service. *GPS Solut.* **2021**, *25*, 142. [[CrossRef](#)]
26. Ren, Z.; Gong, H.; Peng, J.; Tang, C.; Huang, X.; Sun, G. Performance Assessment of Real-Time Precise Point Positioning Using BDS PPP-B2b Service Signal. *Adv. Space Res.* **2021**, *68*, 3242–3254. [[CrossRef](#)]
27. Tu, R.; Zhang, P.; Zhang, R.; Liu, J.; Lu, X. Modeling and Performance Analysis of Precise Time Transfer Based on BDS Triple-Frequency Un-Combined Observations. *J. Geod.* **2019**, *93*, 837–847. [[CrossRef](#)]
28. Li, X.; Huang, J.; Li, X.; Lyu, H.; Wang, B.; Xiong, Y.; Xie, W. Multi-Constellation GNSS PPP Instantaneous Ambiguity Resolution with Precise Atmospheric Corrections Augmentation. *GPS Solut.* **2021**, *25*, 107. [[CrossRef](#)]
29. Ge, Y.; Ding, S.; Qin, W.; Zhou, F.; Yang, X.; Wang, S. Performance of Ionospheric-Free PPP Time Transfer Models with BDS-3 Quad-Frequency Observations. *Measurement* **2020**, *160*, 107836. [[CrossRef](#)]
30. Lyu, D.; Zeng, F.; Ouyang, X.; Zhang, H. Real-Time Clock Comparison and Monitoring with Multi-GNSS Precise Point Positioning: GPS, GLONASS and Galileo. *Adv. Space Res.* **2020**, *65*, 560–571. [[CrossRef](#)]
31. Wu, J.T.; Wu, S.C.; Haji, G.A.; Bertiger, W.I.; Lichten, S.M. Effects of Antenna Orientation on GPS Carrier Phase. *Manuscr. Geod.* **1993**, *8*, 91–98.
32. Gerard, P.; Brian, L. *IERS Conventions (2010)*; BIPM: Paris, France, 2010; p. 180.
33. Davis, J.L.; Herring, T.A.; Shapiro, I.I.; Rogers, A.E.E.; Elgered, G. Geodesy by Radio Interferometry: Effects of Atmospheric Modeling Errors on Estimates of Baseline Length. *Radio Sci.* **1985**, *20*, 1593–1607. [[CrossRef](#)]
34. Boehm, J.; Niell, A.; Tregoning, P.; Schuh, H. Global Mapping Function (GMF): A New Empirical Mapping Function Based on Numerical Weather Model Data. *Geophys. Res. Lett.* **2006**, *33*, L07304. [[CrossRef](#)]
35. Tao, J.; Liu, J.; Hu, Z.; Zhao, Q.; Chen, G.; Ju, B. Initial Assessment of the BDS-3 PPP-B2b RTS Compared with the CNES RTS. *GPS Solut.* **2021**, *25*, 131. [[CrossRef](#)]
36. Zhixi, N.; Xiaofei, X.; Zhenjie, W.; Jun, D. Initial Assessment of BDS PPP-B2b Service: Precision of Orbit and Clock Corrections, and PPP Performance. *Remote Sens.* **2021**, *13*, 2050. [[CrossRef](#)]
37. Tang, C.; Hu, X.; Zhou, S.; Liu, L.; Pan, J.; Chen, L.; Guo, R.; Zhu, L.; Hu, G.; Li, X.; et al. Initial Results of Centralized Autonomous Orbit Determination of the New-Generation BDS Satellites with Inter-Satellite Link Measurements. *J. Geod.* **2018**, *92*, 1155–1169. [[CrossRef](#)]
38. Guo, J.; Xu, X.; Zhao, Q.; Liu, J. Precise Orbit Determination for Quad-Constellation Satellites at Wuhan University: Strategy, Result Validation, and Comparison. *J. Geod.* **2016**, *90*, 143–159. [[CrossRef](#)]
39. Yao, Y.; He, Y.; Yi, W.; Song, W.; Cao, C.; Chen, M. Method for Evaluating Real-Time GNSS Satellite Clock Offset Products. *GPS Solut.* **2017**, *21*, 1417–1425. [[CrossRef](#)]
40. Qin, W.; Ge, Y.; Zhang, Z.; Yang, H.; Su, H.; Yang, X. Enhancing BDS-3 Precise Time Transfer with DCB Modelling. *Measurement* **2021**, *174*, 108641. [[CrossRef](#)]
41. Defraigne, P.; Aerts, W.; Pottiaux, E. Monitoring of UTC(k)'s Using PPP and IGS Real-Time Products. *GPS Solut.* **2015**, *19*, 165–172. [[CrossRef](#)]
42. Parker, T.E.; Zhang, V.; Petit, G.; Yao, J.; Brown, R.C.; Hanssen, J.L. A Three-Cornered Hat Analysis of Instabilities in Two-Way and GPS Carrier Phase Time Transfer Systems. *Metrologia* **2022**, *59*, 035007. [[CrossRef](#)]
43. Defraigne, P.; Bruyninx, C. On the Link between GPS Pseudorange Noise and Day-Boundary Discontinuities in Geodetic Time Transfer Solutions. *GPS Solut.* **2007**, *11*, 239–249. [[CrossRef](#)]
44. Ge, Y.; Zhou, F.; Dai, P.; Qin, W.; Wang, S.; Yang, X. Precise Point Positioning Time Transfer with Multi-GNSS Single-Frequency Observations. *Measurement* **2019**, *146*, 628–642. [[CrossRef](#)]
45. Teunissen, P.J.G.; Odolinski, R.; Odijk, D. Instantaneous BeiDou+GPS RTK Positioning with High Cut-off Elevation Angles. *J. Geod.* **2014**, *88*, 335–350. [[CrossRef](#)]